Contents lists available at SciVerse ScienceDirect

Optics & Laser Technology

High-speed bipolar phototransistors in a 180 nm CMOS process

P. Kostov *, W. Gaberl, H. Zimmermann

Institute of Electrodynamics, Microwave and Circuit Engineering, Vienna University of Technology, Gusshausstr. 25/354, 1040 Vienna, Austria

ARTICLE INFO

ABSTRACT

Several high-speed pnp phototransistors built in a standard 180 nm CMOS process are presented. The phototransistors were implemented in sizes of $40 \times 40\ \mu m^2$ and $100 \times 100\ \mu m^2$. Different base and emitter areas lead to different characteristics of the phototransistors. As starting material a p^+ wafer with a p^- epitaxial layer on top was used. The phototransistors were optically characterized at wavelengths of 410, 675 and 850 nm. Bandwidths up to 92 MHz and dynamic responsivities up to 2.95 A/W were achieved. Evaluating the results, we can say that the presented phototransistors are well suited for high speed photosensitive optical applications where inherent amplification is needed. Further on, the standard silicon CMOS implementation opens the possibility for cheap integration of integrated optoelectronic circuits. Possible applications for the presented phototransistors are low cost high speed image sensors, opto-couplers, etc.

1. Introduction

During the last decades CMOS processes evolved to mature technologies, wherein a cheap implementation of integrated circuits is possible. Compared with III–V compound semiconductors, CMOS technologies have some major advantages like the possibility to combine silicon photodetectors together with the signal processing circuitry into an optoelectronic integrated circuit (OEIC). These single-chip devices exceed assemblies of wire bonded compound photodetectors and integrated circuits in many aspects. One advantage for example is the avoidance of the bond pads and bond wires between photodetector and read out circuitry. This for example leads to an excellent immunity against electromagnetic interference. Other advantages of CMOS OEICs over III–V solutions are the possibility for cheap mass production, easy handling, packaging, etc. [1].

Optical signals are converted into electrical signals by means of photodetectors. The most common photodetectors are photodiodes, phototransistors and avalanche photodiodes. However, phototransistors as well as avalanche photodiodes have the advantage to increase the responsivity compared to simple photodiodes, due to their inherent current amplification.

Silicon photodetectors are able to detect wavelengths between 300 nm and 1100 nm due to the physical properties of the material. Light in the mentioned wavelength range enters the silicon and is absorbed in it. The absorption of the photons leads to the generation of electron–hole pairs with a generation rate G [1]:

$$G(x,\lambda) = \Phi_0 \alpha(\lambda) e^{-\alpha(\lambda)x} \tag{1}$$

The generation rate G is dependent on the wavelength λ the depth x from the semiconductor surface, the photon flux Φ_0 of the incident light and the absorption coefficient α. Light with short wavelength is absorbed near the semiconductor surface, while light in the near infrared region has a larger penetration depth and is therefore absorbed deep in the silicon. For example blue light with a wavelength of 430 nm generates electron–hole pairs in depths up to 0.2 μm while near infrared light with a wavelength of 850 nm has a 1/e penetration depth of about 16.6 μm [1]. Due to the wavelength dependent penetration depth of the light, the photodiodes and phototransistors will also have wavelength dependent bandwidths, since the distribution of the total photocurrent in drift and diffusion part is wavelength dependent. Compound photodetectors, for example InGaAs, InP, or GaAs have due to their material properties higher absorption coefficients α, which lead to small penetration depths in the range up to 1 μm from the surface. However, silicon photodetectors are preferable due to the above described advantages.

Photodiodes can be split into several subcategories. The PN photodiode can be mentioned as the most common photodetector. PN photodiodes consist of a simple p–n junction and are easily integrated into CMOS. This kind of photodiode can be implemented in three different ways. The n-well/p-substrate together with the n^+/p-substrate photodiodes can receive photons of the complete visible and the near infrared spectrum. However, the large 1/e penetration depth of near infrared light leads to long distances which charges

* Corresponding author. Tel.: +43 1 58801 354624; fax: +43 1 58801 9354624.
E-mail addresses: plamen.kostov@tuwien.ac.at (P. Kostov),
wolfgang.gaberl@tuwien.ac.at (W. Gaberl),
horst.zimmermann@tuwien.ac.at (H. Zimmermann).

have to travel in the field free diffusion region. Since the diffusion process is very slow, these kinds of PN diodes are characterized by a small bandwidth. However, the n-well/p-substrate structure has a higher bandwidth and a better responsivity compared to the n^+/p-substrate structure. This is mainly due to the deeper and lower doped n-well layer (compared to n^+), which results in a deeper and also thicker space-charge region. Thus, deep generated electrons have to travel shorter distances to reach the space-charge region, resulting in a higher bandwidth. As a third possibility, an isolated PN photodiode can be built. Thereby a p^+/n-well diode is implemented into the p wafer. Charges which are generated deep in the substrate do not contribute to the photocurrent due to the isolation of the PN diode from the substrate. However, charges generated in the active diode area are rapidly collected, which results in fast detectors, but with low responsivity. An n-well/p-substrate PN photodiode with a bandwidth of 1.6 MHz and a responsivity of 0.5 A/W at 780 nm for a reverse bias voltage of $V_D=5$ V is presented in [2]. In [3] an optical receiver using an n^+/p-substrate photodiode as well as an npn phototransistor built in a 65 nm CMOS process is presented. The paper states a photodiode responsivity of 0.03 A/W and a bandwidth of 2.5 MHz at 850 nm.

PIN photodiodes introduce some orders of magnitude higher bandwidth compared to standard PN photodiodes. They have an additional intrinsic layer between the cathode and anode. In CMOS technologies this low doped epitaxial layer is grown on top of the substrate material. This 10–15 µm thick epi layer leads to a thick space-charge region between the anode and the cathode of the photodiode. By applying a relatively low reverse bias voltage a rather thick drift zone is formed, which results in a large amount of drift current and only a small fraction of diffusion current. As a consequence of the high drift current part, PIN photodiodes achieve very high bandwidths compared to PN diodes. Due to the advantages of PIN diodes over PN diodes, PIN diodes are the most commonly used detectors for high speed optical communication applications like optical receiver [3,4], time-of-flight distance measurement applications [5–8], etc.

However, the responsivity of photodiodes cannot exceed the maximum limited by quantum efficiency $\eta=1$. For example, for a wavelength of 850 nm the responsivity is limited to 0.65 A/W. A maximum quantum efficiency $\eta=1$ cannot be reached in real devices due to reflection of the light at the detector surface as well as recombination of the photogenerated charges in the silicon. Thus in reality the achieved responsivities in reality are smaller and in the range of 0.2 A/W for 410 nm, 0.55 A/W for 675 nm and 0.35 A/W for 850 nm.

Special kinds of photodetectors like avalanche photodiodes and phototransistors can improve the responsivity limitation of the PN and PIN photodiode by an inherent current amplification. By means of their internal amplification they can achieve quantum efficiencies $\eta>1$. Due to this advantage for example the same light source can be used for longer transmission distances compared to PIN and PN photodiodes.

Avalanche photodiodes (APDs) achieve a high amplification of the photocurrent by an inherent avalanche multiplication process. However, the big drawback is the need for a high voltage supply of several tens of volts to achieve sufficient electrical field strength for avalanche amplification [9]. High voltages are a problem in integrated circuits and even more in modern low-voltage processes. However, single-photon avalanche photodiodes (SPADs) are a new kind of avalanche photodiodes, which can operate at smaller bias voltages compared to the described standard avalanche photodiodes. Refs. [10–13] report single-photon avalanche photodiodes with breakdown voltages between 9.4 V and 23.1 V. Another disadvantage of SPADs and APDs is the very narrow bias voltage range for linear operation due to their strongly nonlinear behavior and thus the need for a complex control circuit.

The most important advantage of phototransistors over avalanche photodiodes is that they do not need high voltages for current amplification. Phototransistors can be built in different ways. Some examples for phototransistor implementations in CMOS technologies are vertical bipolar phototransistors [3,14–20], lateral bipolar phototransistors [21] and photo-MOSFETs [22]. The 65 nm CMOS npn phototransistors described in [3] achieve a responsivity of 0.34 A/W and a bandwidth of 150 kHz at 850 nm light. Phototransistors with PIN structure show bandwidths up to 14 MHz and responsivities up to 76 A/W at 675 nm and 37.2 A/W at 850 nm [14]. In [15] a CMOS Lock-In Amplifier using standard CMOS pnp phototransistors with bandwidths of a few hundred kHz is described. Refs. [16,17] report on npn phototransistors with responsivities of 0.25 A/W for the blue spectral range. Another pnp phototransistor with a current gain of 300 and a maximum bandwidth of 7.8 MHz at 638 nm is described in [18]. Some results of this work are presented in [19,20].

2. Working principle

The vertical bipolar pnp phototransistor is formed by the p-substrate, an n-well implant and a p^+ implant inside the n-well. A depiction of the cross-section of such a pnp phototransistor is shown in Fig. 1, wherein the base–collector junction acts as a PN photodiode. Since the collector is formed by the substrate, the pnp phototransistor can only be used in emitter follower configuration. Two space-charge regions are present in the phototransistor, one between the base and the collector and another one between the base and the emitter. Charges generated by the incoming light are separated by the electrical field inside the space-charge regions. Assuming that the base is floating, the electrons are accumulated in the base and makes its potential more negative. The electron accumulation in the base leads to an increase of the base–emitter PN diode forward voltage, which implicates an injection of holes from the emitter into the base. A high portion of the injected holes diffuse through the base and reach the base the base–collector space-charge region. There they are swept into the collector by the electric field. The relation between the collector current I_C and the photocurrent I_{PH} is the inherent current amplification β of the phototransistor.

3. Methodology

In this work we introduce integrated vertical bipolar silicon phototransistors. The phototransistors were implemented in sizes of 40×40 µm^2 and 100×100 µm^2 in a 180 nm standard CMOS
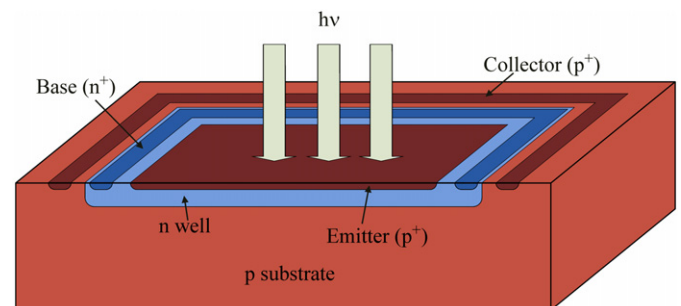

Fig. 1. Cross-section of a common pnp phototransistor integrated in CMOS technology.

process without process modification. A special starting material was used to get a thick space-charge region at the base–collector junction. It consists of a 15 μm thick, low doped (5×10^{13} cm^{-3}) epitaxial grown layer on top of the p-substrate. Due to this p$^-$ epi layer a PIN structure is formed with the advantage of a thick drift zone and thus a large drift current part for deep penetrating light like 850 nm at low voltages. This characteristic leads to a fast separation of the generated electron–hole pairs and furthermore to higher bandwidths compared to standard phototransistors. However, the bandwidth and also the responsivity of the phototransistors are also dependent on the size and design of the base and the emitter area. The characteristics of the phototransistors can be adjusted by changing the base and emitter designs.

3.1. Bandwidth and photocurrent amplification

For speed optimization all implemented phototransistors were built with small emitter areas. The reduction of the emitter size leads to a small base–emitter capacitance C_{BE} and thus to a higher -3 dB bandwidth

$$f_{-3dB} = \frac{1}{2\pi\beta \cdot \left(\tau_B + \frac{k_B T}{qI_E}(C_{BE} + C_{BC})\right)} \qquad (2)$$

where $f_{-3\,dB}$ is the -3 dB bandwidth of the phototransistor, β is the forward current gain of the phototransistor, τ_B is the base transit time, k_B is the Boltzmann constant, T is the absolute temperature, q is the elementary charge, I_E is the emitter current of the phototransistor, C_{BE} is the base–emitter capacitance and C_{BC} is the base–collector capacitance [23].

On the other hand, the small emitter leads also to a reduced responsivity since the photogenerated charges have to travel longer distances to reach the emitter area which increases the probability for recombination. The base of the phototransistor is formed by a homogeneous n-well over the whole photosensitive area (Fig. 2a and b). For a further increase of the bandwidth the base–collector capacitance C_{BC} and thus the base–collector junction area should be reduced. This was done by implementing a second kind of base profile, where the base area was formed only by a small n-well under the emitter area as shown in Fig. 2c and d. A reduction of the perimeter capacitance leads also to a further increase of the bandwidth. Therefore a lateral 3 μm p$^-$ epi layer gap was added between the n-well base and the p-well collector

contact for the devices with a full n-well base. Applying a higher collector–emitter voltage V_{CE} will lead to thicker space-charge regions and thus to smaller base–collector and base–emitter capacitances. This furthermore increases the -3 dB bandwidth. Nevertheless, the bandwidth of phototransistors generally is lower than the bandwidth of PIN photodiodes. This is true on one hand because the phototransistor has two rather high junction capacitances C_{BE} and C_{BC} and on the other hand it is limited by the base transit time τ_B, which is not an issue in a photodiode.

As mentioned before, the responsivity of the phototransistor will be small for a small emitter size due to a higher charge recombination probability. Charges which are not generated directly under the emitter will have to travel longer distances to reach the base–emitter junction. These charges will contribute to the photocurrent if their lifetime is longer than the time they need to reach the emitter. Otherwise they will recombine and get lost. The lifetime of the charge carriers depends on the doping concentration of the base. Furthermore the inherent current amplification of the phototransistor also depends on the doping concentration of the base. A small base doping concentration will lead to a small Gummel number and therefore to a high current amplification. The relation between base doping concentration N_B, Gummel number N_G and inherent current amplification β is shown in Eqs. (3) and (4) [24]:

$$N_G = \int_0^W N_B(x)dx \qquad (3)$$

$$\beta \propto \frac{N_E}{N_G} \qquad (4)$$

where W is the effective width of the base and N_E the emitter doping concentration. The effective width W of the base is the distance between the borders of the base–emitter space-charge region and the base–collector space-charge region inside the base. However, if the effective base width gets too low a reach-through current between collector and emitter can occur. All our implemented phototransistors have a thick enough effective base width to prevent reach-through between the collector and emitter area even for high voltages. This is illustrated by the output characteristic measurements in the measurement results section. As a conclusion we can say that phototransistors for high responsivity should be designed with large emitters over the whole photosensitive area together with a low doped base. However, our
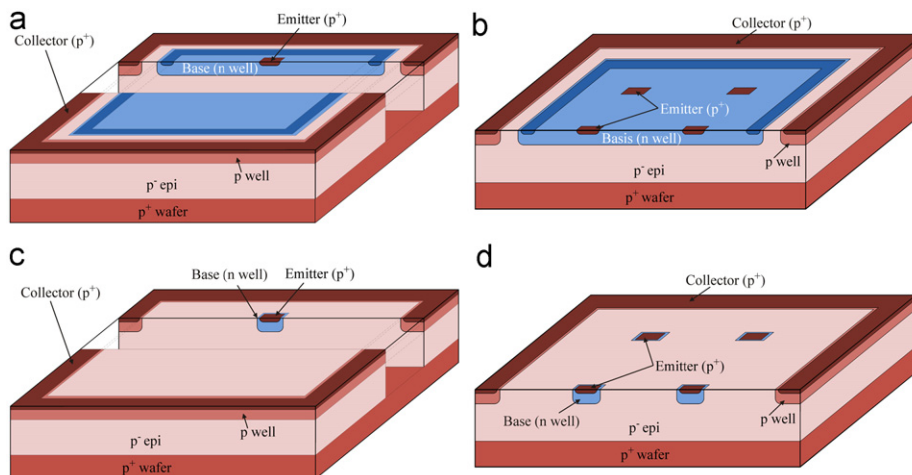

Fig. 2. 3D depiction and cross-section of the four presented phototransistors: (a) PT$_{EDGE}$F$_B$, (b) PT$_{QUAD}$F$_B$, (c) PT$_{EDGE}$S$_B$, and (d) PT$_{QUAD}$S$_B$.

phototransistors are designed primarily for higher bandwidth and therefore they have smaller emitters, with the tradeoff of a reduced responsivity.
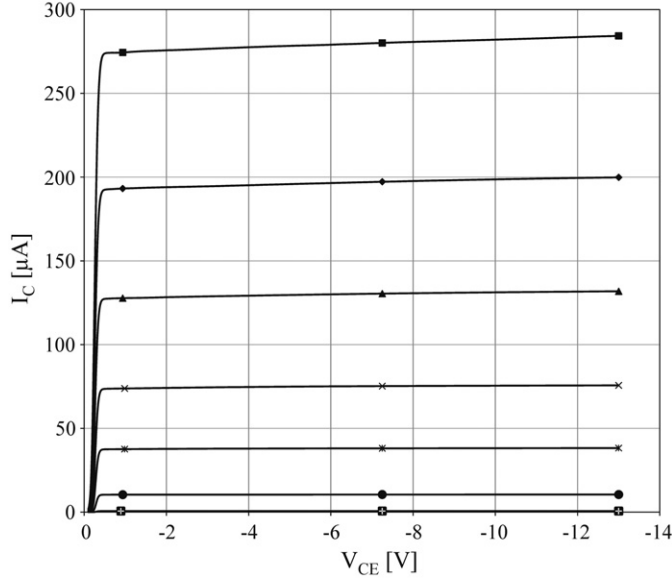

Fig. 3. Output characteristics of the $100 \times 100\ \mu m^2$ $PT_{QUAD}F_B$ phototransistor at 850 nm for different optical powers.

Fig. 4. DC responsivity of the $100 \times 100\ \mu m^2$ $PT_{QUAD}F_B$ phototransistor at 850 nm at $V_{CE} = -10\ V$.

3.2. Phototransistor design

In this work we present four different kinds of phototransistors with different designs of base and emitter area:

- $PT_{EDGE}F_B$
- $PT_{QUAD}F_B$
- $PT_{EDGE}S_B$
- $PT_{QUAD}S_B$

Fig. 2 shows a depiction of the four phototransistors. All phototransistors have the same unique emitter area with a size of $2.18 \times 0.32\ \mu m^2$. PT_{EDGE} phototransistors have their emitter area at the corner of the photosensitive area, wherein PT_{QUAD} phototransistors have their emitter area in the center of each quadrant of the photosensitive area. The idea for having the emitter at the edge of the photosensitive area is based on the idea to have a flat photodetector surface without any contacts. Then it is possible to apply an ARC layer on top of the phototransistors which will lead to an increase of the responsivity by up to 3 dB. On the other hand, for achieving a higher responsivity the four emitter of the PT_{QUAD} were placed in the center of each quadrant of the phototransistor. As described in Section 3.1, the small base (S_B) of the phototransistors was fabricated with the idea to reduce the base–collector capacitance C_{BC} and thus to increase the bandwidth compared to the phototransistors with a full base over the whole photosensitive area (F_B).

4. Measurement results

The presented phototransistors were characterized by optical DC and AC measurements. The output characteristics and DC responsivity were measured by optical DC measurements at 850 nm. Furthermore the spectral responsivity was measured over the whole visible light range and near infrared range. Optical AC measurements were done for acquiring the responsivities, bandwidths and rise times of the phototransistors. The AC measurements were done at three different wavelengths: 410, 675 and 850 nm.
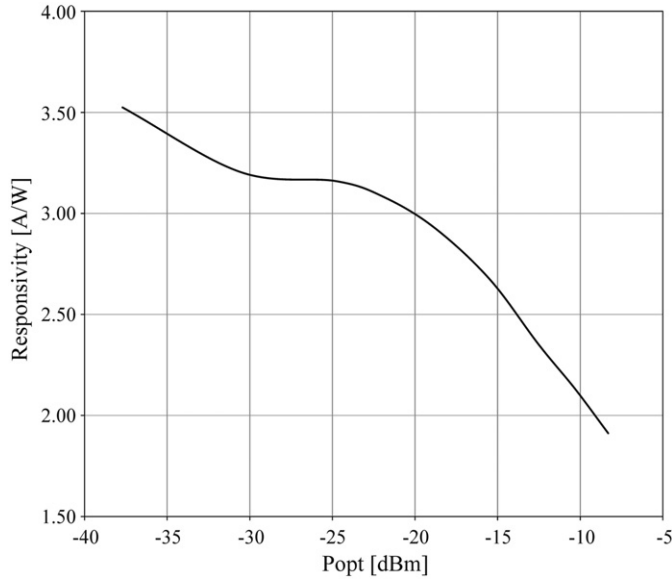
4.1. Optical DC measurements

4.1.1. Output characteristics
The output characteristics of the devices were measured by applying an 850 nm light with different optical light power P_{opt} and varying the collector–emitter voltage V_{CE}. The optical light power P_{opt} was varied thereby from -37.7 dBm to -8.3 dBm. Fig. 3 depicts the output characteristics of the $100 \times 100\ \mu m^2$ $PT_{QUAD}F_B$ phototransistor. As can be seen in Fig. 3 no reach-through occurs for V_{CE} voltages up to $-13\ V$. The output characteristics of the other devices are similar to the presented one.

4.1.2. DC responsivity
In Fig. 4 the calculated DC responsivity at $V_{CE} = -10\ V$ is depicted for the $100 \times 100\ \mu m^2$ $PT_{QUAD}F_B$ phototransistor. It can

Table 1
DC responsivity in A/W for the $100 \times 100\ \mu m^2$ $PT_{EDGE}F_B$ and $PT_{QUAD}F_B$ phototransistors for three different collector–emitter voltages at 850 nm and optical power of -15.5 dBm and -8.3 dBm.

	$P_{opt} = -15.5$ dBm			$P_{opt} = -8.3$ dBm		
	$V_{CE} = -2\ V$	$V_{CE} = -5\ V$	$V_{CE} = -10\ V$	$V_{CE} = -2\ V$	$V_{CE} = -5\ V$	$V_{CE} = -10\ V$
$PT_{EDGE}F_B$	1.99	2.02	2.05	1.34	1.35	1.37
$PT_{QUAD}F_B$	2.63	2.65	2.68	1.87	1.89	1.91

be seen, the responsivity decreases for increased optical light power. This is caused by a reduced gain in the phototransistor. The higher optical light power causes a change of the operating point and thus a different responsivity as described in [14]. As shown in Fig. 3 the collector current I_C has only a minor dependence on V_{CE} in the forward active region of the phototransistor. This leads to a nearly constant responsivity of the device over V_{CE}. Table 1 shows the DC responsivities of the $100 \times 100 \, \mu m^2$ $PT_{EDGE}F_B$ and $PT_{QUAD}F_B$ phototransistors at -2, -5 and $-10 \, V$ and optical light power of -15.5 and $-8.3 \, dBm$.

4.1.3. Spectral responsivity measurements

Spectral responsivity measurements in the range from 400 nm to 900 nm were done using a monochromator. The used monochromator is based on a Spectral Products Xenon Fiber Optic
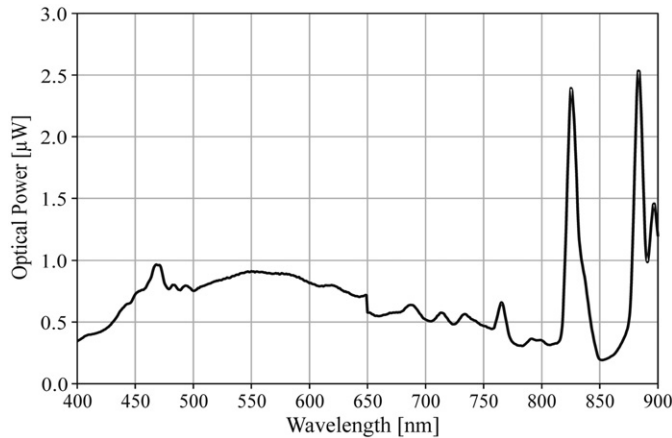
Fig. 5. Emitted optical power of the monochromator used for spectral responsivity measurements.
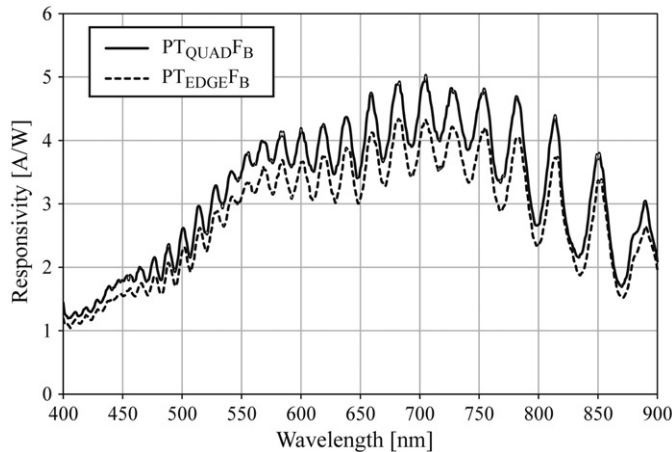
Fig. 6. Spectral responsivity of the $100 \times 100 \, \mu m^2$ $PT_{EDGE}F_B$ and $PT_{QUAD}F_B$ phototransistors.

Lightsource ASB-XE-175, a Spectral Products Digiköm CM110 monochromator and optics for fiber coupling. Furthermore the device has a 50/50 splitter, which allows to monitor the actual output power in parallel to the measurement of the DUT (device under test). The optical power of the monochromator varied between $-35.7 \, dBm$ and $-26 \, dBm$ over the full spectrum (Fig. 5). Fig. 6 depicts the spectral responsivity of the $100 \times 100 \, \mu m^2$ phototransistors $PT_{EDGE}F_B$ and $PT_{QUAD}F_B$ measured at a collector–emitter voltage $V_{CE} = -2 \, V$. The phototransistor with the quad-emitter shows a higher responsivity due to more emitter area and thus less recombination compared to the phototransistor with the edge emitter. A maximal responsivity is measured in the red wavelength range. Furthermore Fig. 6 shows oscillations in the spectral responsivity, which are caused by several oxide layers and one passivation layer. The oxide stack structure can be compared with a Fabry–Perot interferometer, which leads to reflection as well as to transmission dependent on the wavelength. The free spectral range $\Delta\lambda$, which describes the frequency spacing between the responsivity maxima, can be described with the following equation [25]:

$$\Delta\lambda = \frac{\lambda_0^2}{2nd\cos\theta} \tag{5}$$

Here λ_0 is the free-space wavelength, n is the refraction index of the layer, d is the thickness of the layer and θ is the angle of incidence. By applying an ARC layer together with an optical window etch step the oxide stack can be removed and described effects can be eliminated. Nevertheless, the diagrams deviate slightly due to the varying operating point (mean optical power) at different wavelengths.

4.2. Optical AC measurements

The optical AC measurements were done by using modulated light at 410, 675 and 850 nm. For achieving the same collector current I_C, the measurements were done at different optical power for each wavelength. The results at 410 nm were acquired using a laser with an optical light power of $-12.7 \, dBm$ and an extinction ratio of 2. For 675 nm and 850 nm the light power was $-19.2 \, dBm$ and $-15.8 \, dBm$ and the extinction ratio of the laser was 2.74 and 1.48, respectively. Furthermore measurements were taken at different collector–emitter voltages V_{CE}.

4.2.1. AC responsivity

The phototransistors achieve small responsivities due to their small emitter sizes, as already described in Section 3. Based on the fact that charges have to travel longer distances to reach the emitter area, the recombination probability is increased, which leads to a small responsivity. However, the presented phototransistors were designed and optimized for high-speed applications. Table 2 presents the responsivity values for the $40 \times 40 \, \mu m^2$ phototransistors at the three wavelengths and different collector–emitter voltages V_{CE}. The responsivity values for the $100 \times 100 \, \mu m^2$ sized phototransistors have only a minor change compared to the big sized ones. As expected the results show the highest responsivity for red

Table 2
Dynamic responsivity in A/W for the four $40 \times 40 \, \mu m^2$ phototransistors for two different collector–emitter voltages at 410, 675 and 850 nm.

	$\lambda = 410$ nm		$\lambda = 675$ nm		$\lambda = 850$ nm	
	$V_{CE} = -2 \, V$	$V_{CE} = -10 \, V$	$V_{CE} = -2 \, V$	$V_{CE} = -10 \, V$	$V_{CE} = -2 \, V$	$V_{CE} = -10 \, V$
$PT_{EDGE}S_B$	0.48	0.51	2.05	2.18	1.11	1.28
$PT_{EDGE}F_B$	0.64	0.67	1.94	1.97	1.40	1.44
$PT_{QUAD}S_B$	0.67	0.72	2.73	2.95	1.70	1.78
$PT_{QUAD}F_B$	0.86	0.87	2.47	2.63	2.12	2.18

light (675 nm). The maximum achieved responsivity is thereby 2.95 A/W for the $40 \times 40\,\mu m^2$ PT$_{QUAD}$S$_B$ phototransistor at $V_{CE}=-10\,V$.

4.2.2. Bandwidth measurements

The bandwidth of the devices was measured by means of a vector network analyzer (VNA). A depiction of the bandwidth measurement setup is shown in Fig. 7. Phototransistors with a small base (S$_B$) under the emitter area show higher bandwidths

Fig. 7. Setup for frequency response measurements.

than phototransistors with a full base (F$_B$), due to a smaller base–collector capacitance C_{BC}. Furthermore the $40 \times 40\,\mu m^2$ devices show higher bandwidths compared to the $100 \times 100\,\mu m^2$ devices because of a smaller base–collector capacitances C_{BC} as well as a smaller perimeter capacitance. By increasing the collector–emitter voltage V_{CE} both space-charge regions become thicker. This leads to smaller junction capacitances C_{BC} and C_{BE} and as shown in Eq. (2) to a higher bandwidth. In Fig. 8 the dependence of the bandwidth on the phototransistor size together with the collector–emitter voltage V_{CE} is depicted for the phototransistor PT$_{QUAD}$F$_B$ at 675 nm. Table 3 shows the bandwidth values for this phototransistor with both mentioned sizes. In Fig. 9 the measured frequency response of the $40 \times 40\,\mu m^2$ PT$_{EDGE}$S$_B$ phototransistor for the three mentioned wavelengths at a collector–emitter voltage $V_{CE}=-10\,V$ is depicted. This device achieves maximum bandwidths of 60.3, 92.0 and 50.0 MHz at 410, 675 and 850 nm, respectively. Bandwidths for this and the other $40 \times 40\,\mu m^2$ phototransistors at the three wavelengths and different collector–emitter voltages are presented in Table 4. The frequency bandwidth at $V_{CE}=-2\,V$ is noticeable, since the quad emitter devices have a higher bandwidth than the edge emitter devices. This is caused by shorter diffusion distances for generated charges. For all devices the bandwidth maximum is achieved at 675 nm since at this wavelength the main part of the charges is generated in the base–collector space-charge region. All of these charges are directly generated in the electrical field zone. For low collector–emitter voltages $V_{CE}=-2\,V$ the base–collector space charge region will not extend over the whole detector area. Therefore even for 675 nm the device is slow compared to the
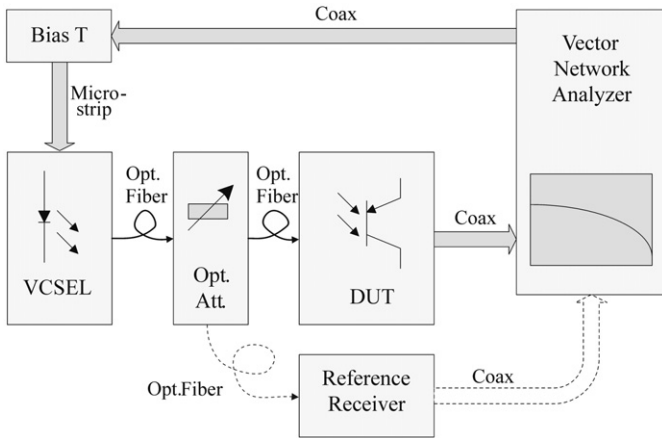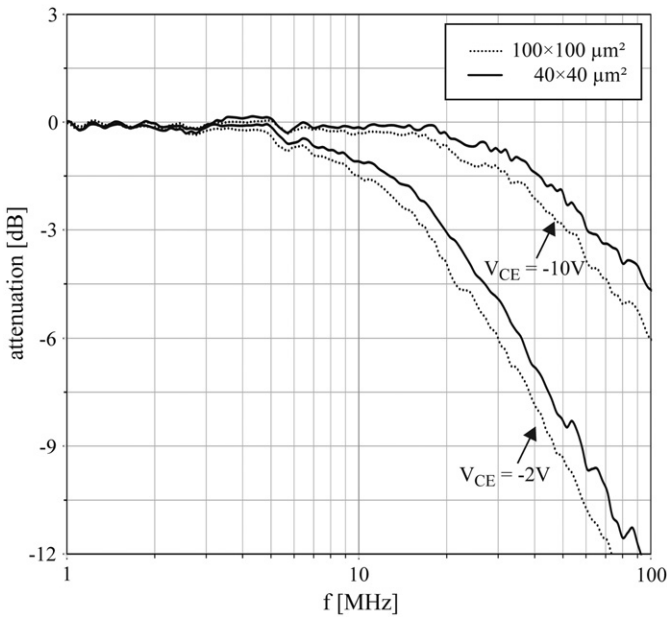

Fig. 8. Frequency response of the $40 \times 40\,\mu m^2$ and $100 \times 100\,\mu m^2$ PT$_{QUAD}$F$_B$ phototransistor at 675 nm and $V_{CE}=-2\,V$ and $-10\,V$.
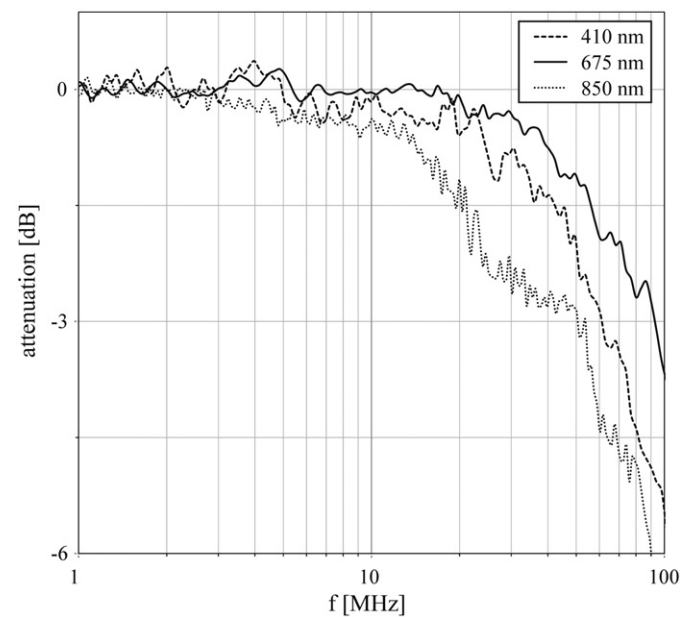

Fig. 9. Frequency response of the $40 \times 40\,\mu m^2$ PT$_{EDGE}$S$_B$ phototransistor at 410, 675, 850 nm and $V_{CE}=-10\,V$.

Table 3
Bandwidth values in MHz for the $40 \times 40\,\mu m^2$ and $100 \times 100\,\mu m^2$ PT$_{QUAD}$F$_B$ phototransistor for two different collector–emitter voltages.

	$\lambda=410$ nm		$\lambda=675$ nm		$\lambda=850$ nm	
	$V_{CE}=-2\,V$	$V_{CE}=-10\,V$	$V_{CE}=-2\,V$	$V_{CE}=-10\,V$	$V_{CE}=-2\,V$	$V_{CE}=-10\,V$
$40 \times 40\,\mu m^2$	20.2	54.2	18.8	60.3	18.6	31.6
$100 \times 100\,\mu m^2$	16.6	34.0	16.1	51.6	15.8	21.4

Table 4
Bandwidth in MHz for the four $40 \times 40\ \mu m^2$ phototransistors for two different collector–emitter voltages at 410, 675 and 850 nm.

	$\lambda = 410$ nm		$\lambda = 675$ nm		$\lambda = 850$ nm	
	$V_{CE} = -2$ V	$V_{CE} = -10$ V	$V_{CE} = -2$ V	$V_{CE} = -10$ V	$V_{CE} = -2$ V	$V_{CE} = -10$ V
$PT_{EDGE}S_B$	13.2	60.3	9.6	92.0	12.0	50.0
$PT_{EDGE}F_B$	12.2	58.6	12.1	77.4	12.8	50.0
$PT_{QUAD}S_B$	20.0	52.0	13.8	72.5	19.1	37.2
$PT_{QUAD}F_B$	20.2	54.2	18.8	60.3	18.6	31.6
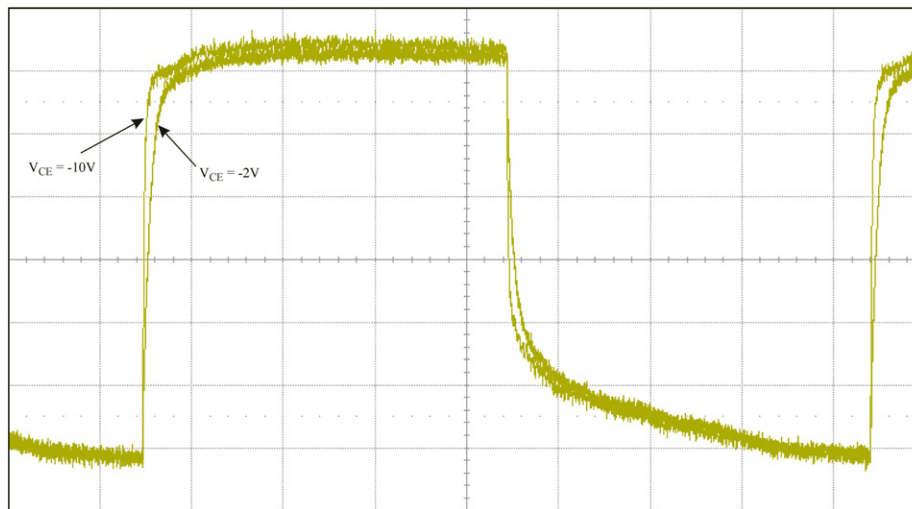
Fig. 10. Step response of the $40 \times 40\ \mu m^2$ $PT_{EDGE}S_B$ phototransistor. Operating point conditions: $P_{opt} = -19$ dBm at 675 nm, $V_{CE} = -2$ V and -10 V. (Axis-properties: x: 200 ns/dev, y: 200 μV/dev).

Table 5
Rise times in ns for the four $40 \times 40\ \mu m^2$ phototransistors for two different collector–emitter voltages at 410, 675 and 850 nm.

	$\lambda = 410$ nm		$\lambda = 675$ nm		$\lambda = 850$ nm	
	$V_{CE} = -2$ V	$V_{CE} = -10$ V	$V_{CE} = -2$ V	$V_{CE} = -10$ V	$V_{CE} = -2$ V	$V_{CE} = -10$ V
$PT_{EDGE}S_B$	27	5	44	12	41	7
$PT_{EDGE}F_B$	20	5	37	15	41	8
$PT_{QUAD}S_B$	16	8	28	13	40	11
$PT_{QUAD}F_B$	17	7	31	19	40	13

higher collector–emitter voltage ($V_{CE} = -10$ V). Nevertheless, for 850 nm the thickness of the whole device is more important than the lateral dimension so phototransistors at low collector–emitter voltages have a higher bandwidth for 850 nm.

4.2.3. Step response measurements

Step response measurements were done for the phototransistors at 410, 675 and 850 nm. Fig. 10 depicts the step function of the $40 \times 40\ \mu m^2$ $PT_{EDGE}S_B$ at $V_{CE} = -2$ V and $V_{CE} = -10$ V. This measurement was done at 675 nm with an optical light power of -19 dBm. The laser was modulated with 630 kHz. Rise times for this device and the other $40 \times 40\ \mu m^2$ phototransistors at different wavelengths and at different collector–emitter voltages are presented in Table 5.

5. Conclusion

In this work we present four kinds of speed optimized bipolar pnp phototransistors built in a standard 180 nm CMOS process without any process modifications. The aim of this work was to design fast devices for deep penetrating light. The increase of the devices' bandwidth was done by reducing the emitter size as well as the base size of the device. The phototransistors were implemented in sizes of $40 \times 40\ \mu m^2$ and $100 \times 100\ \mu m^2$. As starting material a wafer was used with a 15 μm thick low doped p$^-$ epi layer grown on top of the p substrate. By means of this low doped epi layer a thick space-charge region is formed between base and collector which leads to a fast separation of deep generated charges caused by deep penetrating light. The thick space-charge region and thus fast separation of the generated charges are important for achieving high bandwidths. For a further speed optimization the phototransistors were implemented with small emitter areas to reduce the base–emitter capacitance. However, due to the small emitter areas the phototransistors achieve relatively small responsivity values. Nevertheless, the presented phototransistors achieve for 850 nm dynamic responsivities which are by a factor of more than 6 larger than the presented responsivities for the 65 nm pnp phototransistor described in [3].

Table 6
Comparison of CMOS and BiCMOS phototransistor.

Ref.	Technology	Device type	Dimension (μm^2)	V_{CE} (V)	Wavelength (nm)	P_{opt} (dBm)	Responsivity (A/W)	Rise time (ns)	$f_{-3\,dB}$ (MHz)	RBW (A/W*MHz)
[3]	65 nm CMOS	NPN	60×60	1.3	850	×	0.34	×	0.15	0.05
[14]	0.6 μm CMOS	PNP	100×100	−10	850	−10	1.62	25	14[a]	25.2
[15]	0.35 μm CMOS	PNP	35×35	×	×	×	×	×	< 1	×
[16]	×	NPN	700×700	5	420	×	0.25	×	×	×
[18]	0.8 μm BiCMOS	NPN	53×53	×	638	×	×	56	7.8	×
[20]	0.8 μm, 1.2 μm, 2.0 μm CMOS	PNP	60×60	×	660	×	×	3100	×	×
This work	0.18 μm CMOS	PNP	40×40	−10	410	−12.7	0.51	5	60.3[a]	30.8
					675	−19.2	2.18	12	92.0[a]	200.1
					850	−15.8	1.28	7	50.0[a]	64.0

[a] Fastest device.

Furthermore, the presented phototransistors achieve bandwidths up to 60 MHz for 410 nm, up to 92 MHz for 675 nm and up to 50 MHz for 850 nm. When comparing the bandwidth results for 850 nm with the results of the phototransistor presented in [3], the bandwidth increase is more than a factor of 330. Alternatively compared to the fastest own results presented in [14] the bandwidth increase is still a factor of more than 3 at 850 nm. A globally optimized phototransistor cannot be found, since its properties and its realization depend strongly on the demands on the application field. A trade-off between responsivity and bandwidth exists and thus each phototransistor can only be the best solution for a narrow field of application. Furthermore, the phototransistors are hard to be compared meaningfully with other devices (even other phototransistors) due to their strongly non-linear behavior. The nonlinearity leads to a strong dependence on different factors like collector–emitter voltage, wavelength, size of the device, optical light power, additional base currents, etc. Unfortunately many publications on phototransistors are lacking one or more of these values, which gives them limited comparability. However, in Table 6 we have tried to give a comparison of the fastest presented device together with other (Bi)CMOS phototransistors from literature. Due to the presented results these phototransistors are well suited for cheap high speed optical CMOS applications, where a photosensitive device with an inherent current amplification is needed for weak light detection. Possible applications are fast opto-coupler, optical data receiver, etc.

Acknowledgments

References

[1] Zimmermann H. Integrated silicon optoelectronics. 2nd ed. Berlin, Heidelberg: Springer-Verlag; 2010.
[2] Fullin E, Voirin G, Chevroulet M, Lagos A, Moret JM. CMOS-based technology for integrated optoelectronics: a modular approach. IEEE International Electron Devices Meeting 1994:527–30.
[3] Carusone AC, Yasotharan H, Kao T. CMOS technology scaling considerations for multi-gbps optical receivers with integrated photodetectors. IEEE Journal of Solid-State Circuits 2011;46(8):1832–42.
[4] Swoboda R, Zimmermann H. 11Gb/s monolithically integrated silicon optical receiver for 850 nm wavelength. Proceedings of the IEEE international solid-state circuit conference, digest of technical papers ISSCC, vol. 49. 2006. pp. 240–1.
[5] Nemecek A, Oberhauser K, Zimmermann H. Correlating PIN-photodetector with novel difference-integrator concept for range-finding applications. Proceedings of ESSCIRC, european solid-state circuits conference. 2005. pp. 491–4.
[6] Davidovic M, Zach G, Schneider-Hornstein K, Zimmermann H. Range finding sensor in 90 nm CMOS with bridge correlator based background light suppression. Proceedings of ESSCIRC, european solid-state circuit research conference. 2010. pp. 298–301.
[7] Zach G, Zimmermann H. A 2×32 range-finding sensor array with pixel-inherent suppression of ambient light up to 120klx. Proccedings of the IEEE international solid-state circuit conference, digest of technical papers ISSCC, vol. 52. 2009. pp. 352–4.
[8] Zach G, Davidovic M, Zimmermann H. Extraneous-light resistant multipixel range sensor based on a low-power correlating pixel-circuit. Proceedings of ESSCIRC, european solid-state circuits conference. 2009. pp. 236–9.
[9] Cova S, Ghioni M, Lacaita A, Samori C, Zappa F. Avalanche photodiodes and quenching circuits for single-photon detection. Applied Optics 1996;35(12):1956–1976.
[10] Gersbach M, Richardson J, Mazaleyrat E, Hardillier S, Niclass C, Henderson R, et al. A low-noise single-photon detector implemented in a 130 nm CMOS imaging process. Solid State Electronics 2009;53:803–8.
[11] Karimi MA, Gersbach M, Charbon E. A new single-photon avalanche diode in 90 nm standard CMOS technology. Proceedings of SPIE—The International Society for Optical Engineering 2010;7780 art. no. 77801F.
[12] Richrdson J, Grant LA, Webster EAG, Henderson R. A 2 μm diameter, 9 Hz dark count, single photon avalanche diode in 130 nm CMOS technology. Proceedings of ESSDERC, european solid-state device research conference. 2010. pp. 257–60.
[13] Pancheri L, Stoppa D. Low-noise single photon avalanche diodes in 0.15 μm CMOS technology. Proceedings of ESSDERC, european solid-state device research conference. 2011. pp. 179–82.
[14] Kostov P, Schneider-Hornstein K, Zimmermann H. Phototransistors for CMOS optoelectronic integrated circuits. Sensors and Actuators: A Physical 2010. http://dx.doi.org/10.1016/j.sna.2011.03.056.
[15] Hu A, Chodavarapu VP. CMOS optoelectronic lock-in amplifier with integrated phototransistor array. IEEE Transactions on Biomedical Circuits and Systems 2010;4(5):274–80.
[16] Tibuzzi A, Dalla Betta GF, Piemonte C, Di Natale C, D'Amico A, Soncini G. High gain bipolar junction phototransistors with finger-shaped emitter for improved optical gas sensing in the blue spectral region. Sensors and Actuators A 2007;136:588–96.
[17] Tibuzzi A, Dalla Betta GF, Ficorella F, Soncini G, Di Natale C D'Amico A, et al. Finger emitter/base bipolar junction phototransistors for optical gas sensing in the blue spectral region. Proceedings of IEEE sensors, vol. 3, art. no. W3L-F.2. 2004. pp. 1581–4.
[18] Kieschnick K, Zimmermann H, Seegebrecht P. Silicon-based optical receivers in BiCMOS technology for advanced optoelectronic integrated circuits. Materials Science in Semiconductor Processing 2000;3:395–8.
[19] Kostov P, Gaberl W, Zimmermann H. High-speed PNP PIN phototransistors in a 0.18 μm CMOS process. IEEE ESSDERC 2011:187–90.
[20] Kostov P, Gaberl W, Polzer A, Zimmermann H. CMOS PIN phototransistors for high-speed photosensitive applications. Procedia Engineering 2011;25:1397–1400.
[21] Sandage RW, Connelly JA. A fingerprint opto-detector using lateral bipolar phototransistors in a standard CMOS process. IEEE International Electron Devices Meeting 1995:171–4.
[22] Zhang W, Chan M, Ko PK. A novel high-gain CMOS image sensor using floating N-well/gate tied PMOSFET. IEEE International Electron Devices Meeting 1998:1023–5.
[23] Winstel G, Weyrich C. Optoelektronik II. Berlin, Heidelberg: Springer; 1986 p. 97.
[24] Sze SM, Ng KK. Physics of semiconductor devices. 3rd ed. New York: Wiley; 2006.
[25] Reider GA. Photonik. 2nd ed. Wien: Springer-Verlag; 1997.